*Inorg. Chem.* **2007**, *46*, 625–637


# Selective Self-Assembly of Hexameric Homo- and Heteropolymetallic Lanthanide Wheels: Synthesis, Structure, and Photophysical Studies

**Xiao-Yan Chen,[†] Yann Bretonnière,[†] Jacques Pécaut,[†] Daniel Imbert,[‡] Jean-Claude Bünzli,[‡] and Marinella Mazzanti*[,†]**

*Laboratoire de Reconnaissance Ionique et Chimie de Coordination, Service de Chimie Inorganique et Biologique (UMR-E 3 CEA-UJF), Département de Recherche Fondamentale sur la Matière Condensée SCIB/DRFMC/DSM CEA-Grenoble, 17 rue des Martyrs 38054 Grenoble, Cedex 09, France, and Swiss Federal Institute of Technology, Lausanne Laboratory of Lanthanide Supramolecular Chemistry BCH 1402, CH-1015 Lausanne, Switzerland*

Received September 22, 2006

A rational approach to the formation of pure heteropolymetallic lanthanide complexes that uses a two-step assembly strategy and exploits the different size requirements of the two metals included in the final structure is described. The investigation of the assembly of $[LnL_2](Otf)$ (L = 2,2′:6′,2″-terpyridine-6-carboxylate) complexes into hexametallic rings hosting an additional hexacoordinated lanthanide cation was crucial for the development of this strategy. The formation and size of the cyclic assembly are controlled by the ionic radius and by the coordination number of the lanthanides. The rather high luminescence quantum yield of the heptaeuropium complex (25%) indicates that the ring structure is well adapted to include highly luminescent lanthanide complexes in nanosized architecture. The use of a stepwise synthetic strategy leads to the selective assembly of large heteropolymetallic rings. The addition of a smaller lanthanide ion to the $[EuL_2](Otf)$ complex in anhydrous acetonitrile leads selectively to heterometallic species with the Eu ions located on the peripheral sites and the smaller ion occupying only the central site. The high selectivity is the result of the different size requirements of the two metal sites present in the cyclic structure. The heterometallic structure of the isolated $[Lu\subset(EuL_2)_6](Otf)_9$ complex was confirmed by X-ray diffraction and by high resolution solid-state photophysical studies. The described synthetic approach allowed us to obtain the first example of selective assembly of two different lanthanide ions in a large polymetallic structure characterized in solution and in the solid state and will make the isolation of planned dimetallic combinations presenting different lanthanide emitters in the peripheral sites possible.

## Introduction

The design and the synthesis of lanthanide-containing nanoscale molecules has received increasing attention in the past few years because of potential applications of lanthanide-based systems in phosphors for fluorescent lighting, X-ray imaging, amplifiers for fiber-optic communication, luminescent tags for biological molecules, and contrast agents for magnetic resonance imaging.[1−6]

Although the self-assembly of large polymetallic complexes is less developed for f elements than for the d-metal ions, several coordination chemistry strategies have been found to produce highly sophisticated structures.[7] In particular, the approach to polymetallic lanthanide clusters taking advantage of bridging alkolates, phenolates, or chalcogenolates has been extensively explored[8−11] because of the

* To whom correspondence should be addressed. E-mail: marinella.mazzanti@cea.fr.
† Laboratoire de Reconnaissance Ionique and Chimie de Coordination.
‡ Swiss Federal Institute of Technology.

(1) Tissue, B. M. *Chem. Mater.* **1998**, *10*, 2837−2845.
(2) Livramento, J. B.; Toth, E.; Sour, A.; Borel, A.; Merbach, A. E.; Ruloff, R. *Angew. Chem., Int. Ed.* **2005**, *44*, 1480−1484.
(3) Merbach, A. E.; Toth, E. *The Chemistry of Contrast Agents in Medical Magnetic Resonance Imaging*; Wiley: Chichester, U.K., 2001.
(4) Bünzli, J.-C. G.; Piguet, C. *Chem. Soc. Rev.* **2005**, *34*, 1048−1077.
(5) Piguet, C.; Bünzli, J.-C. G. *Chem. Soc. Rev.* **1999**, *28*, 347−358.
(6) Parker, D.; Williams, J. A. G. *J. Chem. Soc., Dalton Trans.* **1996**, 3613−3628.
(7) Bünzli, J.-C. G.; Piguet, C. *Chem. Rev.* **2002**, *10*, 1897−1928.
(8) Evans, W. J.; Greci, M. A.; Ziller, J. W. *Inorg. Chem.* **2000**, *39*, 3212−3220.
(9) Poncelet, O.; Hubert-Pfalzgraf, L. G.; Daran, J.-C.; Astier, R. *J. Chem. Soc., Chem. Commun.* **1989**, 1846−1848.
(10) Barnhart, D. M.; Clark, D. L.; Gordon, J. C.; Huffman, J. C.; Watkin, J. G.; Zwick, B. D. *J. Am. Chem. Soc.* **1993**, *115*, 8461−8462.

10.1021/ic061806o CCC: $37.00 
Published on Web 12/23/2006

potential application of these complexes as precursor for lanthanide-containing materials.[12] In an alternative approach, high-nuclearity oxo/hydroxo clusters have been assembled via the ligand-controlled hydrolysis of lanthanides.[13−16] Very little information is however available in both cases on the structure of the species present in solution, rendering it difficult to rationalize and therefore predict their formation. The strategy relying on the predetermined self-assembly of multistranded helicates through the rational design of multidentate N-donor ligands has been successfully used to prepare, usually, dimetallic[17,18] and, more rarely, trimetallic[19] and tetrametallic[20] lanthanide edifices. Thorough thermodynamic solution studies have allowed the rationalization of the assembly process of homometallic and heterometallic lanthanide helicates.[19,21,22] The self-assembly of sophisticated architectures has also been achieved by using tripodal $C_3$-symmetric polydentate ligands.[23,24] More recently three examples have been described in which simple tridentate or tetradentate asymmetric ligands are used to produce large lanthanide clusters or wheels hosting one or two lanthanide ions.[25−27] High-nuclearity ring complexes are well-known for 3d-transition metals,[28] but only few examples of such intriguing structures have been reported for lanthanide ions.[9,26,29−33] Although an important role of the encapsulated cation can be anticipated in the three systems cited above, the lack of information on the solution structures of the nonalanthanide cluster assembled with the help of a bipyridine bearing a phosphonic acid group[27] and of the octameric ellipsoid lanthanide complexes assembled by a tridentate carboxamidopicolinate prevents a deeper understanding of the assembly process. In a preliminary work,[25] the formation of an hexameric europium wheel encapsulating an europium cation in its center in presence of a tetradentate terpyridinecarboxylate ligand was monitored in solution. In this paper, we describe a two-step synthetic procedure for the selective assembly of pure large heteropolymetallic wheels containing two different lanthanide ions. The inclusion of different f elements in one molecular edifice presents a high fundamental interest for understanding energy-transfer processes.[7,34] Intermetallic exchanges could be used to induce new optical and magnetic properties in doped solids and molecular complexes leading to the development of novel materials. For example, a careful choice of the metal ions can yield lanthanide-sensitized lanthanide luminescence[35] or dual emission in the visible and NIR range.[27] Selective recognition of two different $Ln^{III}$ ions in a polymetallic assembly is extremely challenging because of their very similar coordination behavior and relies on the small differences in size along the lanthanide series.[21] NMR and ESI-MS investigation on the formation of heterodimetallic and heterotrimetallic lanthanide helicates in solution showed significant deviation from statistical distribution.[21,36] However, only very few examples are reported describing the isolation of pure heterobimetallic Ln−Ln complexes in the solid state, and they are limited to bimetallic assemblies.[37−40] Pure heterobimetallic (4f-4f′) complexes were prepared with a tripodal ligand containing two different coordination sites using a stepwise synthetic procedure although the solution structure of these species was not elucidated.[41] Magnetic studies of these dimetallic complexes have allowed the first detection and characterization of the interactions between f-electronic systems.[39] Attempts to introduce different lanthanide ions in large polymetallic complexes are fewer in spite of the anticipated luminescence properties. Significant deviations from the statistical distribution have been reported for pentametallic nano clusters which have been characterized only in the solid state.[42] In this work, we describe the first example of selective assembly of large heterometallic wheels which are characterized both in solution and in the solid state. The selective formation of the heptametallic hetero-lanthanide wheel is controlled by the size of the cation acting


(11) Banerjee, S.; Huebner, L.; Romanelli, M. D.; Kumar, G. A.; Riman, R. E.; Emge, T. J.; Brennan, J. G. *J. Am. Chem. Soc.* **2005**, *127*, 15900−15906.
(12) Hubert-Pfalzgraf, L. G. *Inorg. Chem. Commun.* **2003**, *6*, 102−120.
(13) Zheng, Z. *Chem. Commun.* **2001**, 2521−2529.
(14) Wang, R.; Song, D.; Wang, S. *Chem. Commun.* **2002**, 368−369.
(15) Xu, G.; Wang, Z. M.; He, Z.; Lu, Z.; Liao, C. S.; Yan, C. H. *Inorg. Chem.* **2002**, *41*, 6802−6807.
(16) Wang, R. Y.; Selby, H. D.; Liu, H.; Carducci, M. D.; Jin, T. Z.; Zheng, Z. P.; Anthis, J. W.; Staples, R. J. *Inorg. Chem.* **2002**, *41*, 278−286.
(17) Piguet, C.; Bernardinelli, G.; Hopfgartner, G. *Chem. Rev.* **1997**, *97*, 2005−2062.
(18) Albrecht, M. *Chem. Rev.* **2001**, *101*, 3457.
(19) Floquet, S.; Ouali, N.; Bocquet, B.; Bernardinelli, G.; Imbert, D.; Bünzli, J.-C. G.; Hopfgartner, G.; Piguet, C. *Chem.−Eur. J.* **2003**, *9*, 1860−1875.
(20) Zeckert, K.; Hamacek, J.; Senegas, J. M.; Dalla-Favera, N.; Floquet, S.; Bernardinelli, G.; Piguet, C. *Angew. Chem., Int. Ed.* **2005**, *44*, 7954−7958.
(21) Floquet, S.; Borkovec, M.; Bernardinelli, G.; Pinto, A.; Leuthold, L. A.; Hopfgartner, G.; Imbert, D.; Bünzli, J.-C. G.; Piguet, C. *Chem.−Eur. J.* **2004**, *10*, 1091−1105.
(22) Zeckert, K.; Hamacek, J.; Rivera, J. P.; Floquet, S.; Pinto, A.; Borkovec, M.; Piguet, C. *J. Am. Chem. Soc.* **2004**, *126*, 11589−11601.
(23) Xu, J.; Raymond, K. N. *Angew. Chem., Int. Ed. Engl.* **2000**, *39*, 2745−2747.
(24) Bretonnière, Y.; Mazzanti, M.; Wietzke, R.; Pécaut, J. *Chem. Commun.* **2000**, 1543−1544.
(25) Bretonniere, Y.; Mazzanti, M.; Pecaut, J.; Olmstead, M. M. *J. Am. Chem. Soc.* **2002**, *124*, 9012−9013.
(26) Hou, H.; Wei, Y.; Song, Y.; Fan, Y.; Zhu, Y. *Inorg. Chem.* **2004**, *43*, 1323−1327.
(27) Comby, S.; Scopelliti, R.; Imbert, D.; Charbonnière, L. J.; Ziessel, R.; Bünzli, J.-C. *Inorg. Chem.* **2006**, *45*, 3158−3160.
(28) Winpenny, R. E. P. *Transition Metals in Supramolecular Chemistry*; John Wiley & Sons: Chichester, U.K., 1999; Vol. 5.
(29) Kajiwara, T.; Wu, H. S.; Ito, T.; Iki, N.; Miyano, S. *Angew. Chem., Int. Ed.* **2004**, *43*, 1832−1835.
(30) Westin, L. G.; Kritikos, M.; Caneschi, A. *Chem. Commun.* **2003**, 1012−1013.
(31) Gamer, M. T.; Roesky, P. W. *Inorg. Chem.* **2005**, *44*, 5963−5965.
(32) Ganesan, M.; Gambarotta, S.; Yap, G. P. A. *Angew. Chem., Int. Ed.* **2001**, *40*, 766−769.
(33) Anwander, R. *Angew. Chem., Int. Ed. Engl.* **1998**, *37*, 599−602.
(34) Matthews, K. D.; Fairman, R. A.; Johnson, A.; Spence, K. V. N.; Kahwa, I. A.; McPherson, G. L.; Robotham, H. *J. Chem. Soc., Dalton Trans.* **1993**, 1719−1723.
(35) Faulkner, S.; Pope, S. J. A. *J. Am. Chem. Soc.* **2003**, *125*, 10526−10527.
(36) André, N.; Scopelliti, R.; Hopfgartner, G.; Piguet, C.; Bünzli, J.-C. *Chem. Commun.* **2002**, *214*.
(37) Ishikawa, N.; Iino, T.; Kaizu, Y. *J. Am. Chem. Soc.* **2002**, *124*, 11440−11447.
(38) Gross, T.; Chevalier, F.; Lindsey, J. S. *Inorg. Chem.* **2001**, *40*, *4762*.
(39) Costes, J. P.; Nicodeme, F. *Chem.−Eur. J.* **2002**, *8*, 3442−3447.
(40) Costes, J. P.; Clemente-Juan, M. J.; Dahan, F.; Nicodeme, F.; Verelst, M. *Angew. Chem., Int. Ed.* **2002**, *41*, 323−325.
(41) Costes, J. P.; Dahan, F.; Dupuis, A.; Lagrave, S.; Laurent, S. *Inorg. Chem.* **1998**, *37*, 153.
(42) Thompson, M. K.; Lough, A. J.; White, A. J. P.; Williams, D. J.; Kahwa, I. A. *Inorg. Chem.* **2003**, *42*, 4828−4841.

as a template. In addition, the heterometallic $[Lu\subset(EuL_2)_6](Otf)_9$ complex has been fully characterized by X-ray diffraction, NMR, and high-resolution photophysical studies.

## Experimental Section

**General Information.** All manipulations of the lanthanide complexes were carried out under an inert argon atmosphere using Schlenk techniques and a Braun glovebox equipped with a purifier unit (unless otherwise stated). The solvents, purchased from Aldrich in their anhydrous forms, were transferred into a Schlenk flask under an argon atmosphere and were vacuum distilled from K (diisopropylether) or from $CaH_2$, after refluxing 72 h (acetonitrile and deuterated acetonitrile). Anhydrous methanol was purchased from Aldrich and used without further purification. Starting materials were purchased from Aldrich, Fluka, and Alfa and used without further purification unless otherwise stated. $Ln(Otf)_3$ salts were purchased from Aldrich. Residual water present in these salts was removed by heating at 120 °C under vacuum ($10^{-2}$ mmHg) for one week. The 6-methyl-2,2′:6′,2″-terpyridine was prepared from 2-acetyl-6-picoline as previously described.[43,25]

**6,2′:6′,2″-terpyridine-2-carboxylic acid (LH).** Selenium dioxide (21.5 g, 12 equiv) was added to a solution of 6-methyl-2,2′:6′,2″-terpyridine (4 g, 16.2 mmol) in pyridine (100 mL). The mixture was refluxed for 5 days and then filtered through Celite while it was still hot. The resulting solution was evaporated under reduced pressure, and the residue was dissolved in water. The pH was adjusted to 3 with concentrated hydrochloric acid. After the mixture was cooled, a yellow solid formed, which was filtered and recrystallized from a water/ethanol (1:1) mixture to give $LH{\cdot}H_2O$ (3.45 g, 77% yield). The final compound contains traces of unreacted selenium dioxide. Anal. Calcd for $C_{16}H_{11}N_3O_2$: C, 65.08; H, 4.40; N, 14.23. Found: C, 65.22; H, 4.38; N, 14.19.

The water contained in the ligand was removed by heating at ~80 °C under vacuum ($10^{-2}$ mmHg) for one week prior to reaction with the lanthanide salts.

$^1$H NMR (DMSO-$d_6$): $\delta$ 8.84 (dd, $H_3$, $J_{3-4} = 7.6$ Hz, $J_{3-5} = 1.2$ Hz), 8.73 (ddd, $H_{6''}$, $J_{6''-5''} = 4.7$ Hz, $J_{6''-4''} = 1$ Hz, $J_{6''-3''} = 1$ Hz), 8.64 (dt, $H_{3''}$, $J_{3''-4''} = 8.4$ Hz, $J_{3''-5} = 1$ Hz), 8.61 and 8.48 (dd + dd, $H_{3'}$ and $H_{5'}$, $J_{3'-4'} = 7.8$ Hz, $J_{4'-5'} = 7.8$ Hz, $J_{3'-5'} = 1$ Hz), 8.20 (t, $H_4$, $J_{4-5} = 7.6$ Hz), 8.15 (t + d, 2H, $H_5 + H_{4'}$), 8.02 (td, $H_{4''}$, $J_{4''-5''} = 7.7$ Hz), 7.50 (ddd, $H_{5''}$). $^{13}$C NMR (DMSO-$d_6$): $\delta$ 121.7 $C_{3''}$, 122.0 and 122.2 $C_{3'}$ and $C_{5'}$, 124.8 $C_3$, 125.4 $C_{5''}$, 125.9 $C_5$, 138.3 $C_{4''}$, 139.6 $C_{4'}$, 139.8 $C_4$, 148.8 $C_{6''}$, 150.2, 154.9, 154.8, and 154.5 $C_{quaternary}$, 156 $C_6$, 166.8 COO. ES$^+$-MS: *m*/*z* 278.3 $[L + H]^+$, 300.4 $[L + Na]^+$.

**Lanthanides Complexes. $[LnL_2](Otf)$ (Ln = Eu, 1; Gd, 2; Tb, 3; Nd, 4).** Triethylamine (71.3 $\mu$L, 0.5 mmol) was added to a suspension of 2,2′:6′,2″-terpyridine-2-carboxylic acid (140 mg, 0.50 mmol) in methanol (15 mL). The reaction mixture was stirred at room temperature for a few hours. When necessary, the resulting yellow solution was filtered to eliminate traces of selenium dioxide (small ligand impurity). $Ln(Otf)_3$ (0.25 mmol) was then added to the resulting yellow solution, and the mixture was first heated at 50° for 10 min and then stirred for 30 min. Diethyl ether was added to the resulting solution. After 24 h at room temperature, a white solid formed, which was filtered, digested in minimal amounts of acetonitrile (to eliminate traces of methanol, ether, and residual water), filtered, and dried under reduced pressure for 24 h to yield the complexes $[LnL_2](Otf)$ (Ln = Eu, **1**; Gd, **2**; Tb, **3**; Nd, **4**) (70% yield).

**Scheme 1**

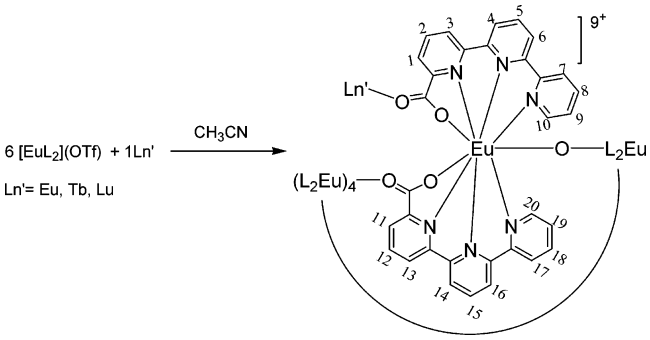


$^1$H NMR (400 MHz, $CD_3OD$, 298 K): $\delta$ 15.70 (broad s, $H_{6''}$), 9.02 (t, $H_{4'}$), 8.65 (t, $H_{5'}$), 7.03 (t, $H_4$), 6.82 (d, $H_{3''}$), 6.40 (d, $H_{3'}$), 6.27 (s, $H_{4''}$), 5.97 (d, $H_5$), 5.70 (d, $H_3$), 1.37 (broad s, $H_{5''}$). Anal. Calcd for $[EuL_2]Otf{\cdot}H_2O$, $C_{33}H_{22}EuN_6F_3O_8S$: C, 45.47; H, 2.54, N, 9.64. Found (analysis performed in air): C, 45.11; H, 2.60; N, 9.57. ES$^+$-MS: *m*/*z*: 705.1 $[EuL_2]^+$. Anal. Calcd for $[GdL_2](Otf){\cdot}H_2O$, $C_{33}H_{22}EuN_6F_3O_8S$: C, 45.20; H, 2.29; N, 9.58; Gd, 17.90. Found: C, 45.16; H, 2.28; N, 9.36; Gd, 17.45. Anal. Calcd for $[NdL_2](Otf){\cdot}H_2O$, $C_{33}H_{22}NdN_6F_3O_8S$: C, 45.88; H, 2.33; N, 9.72; Nd, 17.05. Found: C, 45.71; H, 2.22; N, 9.72; Nd, 16.78. Anal. Calcd for $[TbL_2](Otf)$, $TbC_{33}H_{20}N_6F_3O_7S$: C, 46.18; H, 2.33; N, 9.78. Found (analysis performed under argon on a dried sample): C, 45.84; H, 2.10; N, 9.69. Anal. Calcd for $[EuL_2](Otf)$, $EuC_{33}H_{20}N_6F_3O_7S$: C, 46.44; H, 2.36; N, 9.84. Found (analysis performed under argon on a dried sample): C, 45.96; H, 2.49; N, 10.01.

**$[Ln\subset(LnL_2)_6](Otf)_9$ (Ln = Eu, 5; Nd, 6; Gd, 7; Tb, 8).** $Ln(Otf)_3$ (0.014 mmol) was added to a suspension of $[LnL_2](Otf)$ (0.088 mmol) in acetonitrile (3 mL). The reaction mixture was stirred and heated (~70 °C) until dissolution of the solid (for about 10 min). The resulting solution was filtered, and diisopropylether (3 mL) was added to produce a microcrystalline white solid (yield 74%). Prolonged drying of the solid sample under vacuum results in the loss of the cocrystallized solvent molecules as shown by elemental analyses of the Tb and Gd complexes. Single crystals suitable for diffraction analysis were grown by slow vapor diffusion of diisopropylether into $10^{-2}$ M acetonitrile solutions of the complexes or by the standing of concentrated ($2 \times 10^{-2}$ M) acetonitrile solutions of the complexes at room-temperature.

**$[Eu\subset(EuL_2)_6](Otf)_9$ (5).** Anal. Calcd for $[Eu\subset(EuL_2)_6](Otf)_9{\cdot}10CH_3CN$ (PM = 6114.6), $C_{221}H_{150}Eu_7N_{46}F_{27}O_{51}S_9$: C, 43.40; H, 2.47; N, 10.53. Found: C, 43.10 H, 2.57 N, 10.28. ES$^+$-MS: *m*/*z* 2410.1$\{[EuL_2]_6(Otf)_4\}^{2+}$, 1556.7$\{[EuL_2]_6(Otf)_3\}^{3+}$, 1130.5 $\{[EuL_2]_6(Otf)_2\}^{4+}$. The proton NMR spectrum (Figure 1) was fully assigned by NOESY and COSY experiments and by comparison with the heteropolymetallic Eu−Lu complex.

**$[Nd\subset(NdL_2)_6](Otf)_9$ (6).** Anal. Calcd for $[Nd\subset(NdL_2)_6](Otf)_9{\cdot}10CH_3CN$ (PM = 5811), $Nd_7C_{203}H_{123}N_{37}F_{27}O_{51}S_9$: C, 42.72: H, 2.17; N, 9.08. Found: C, 41.78 H, 2.13 N, 8.90. ES$^+$-MS: *m*/*z* 1538.8 $\{[NdL_2]_6(Otf)_3\}^{3+}$, 1118.6 $\{[NdL_2]_6(Otf)_2\}^{4+}$.

**$[Gd\subset(GdL_2)_6](Otf)_9$ (7).** Anal. Calcd for $[Gd\subset(GdL_2)_6](Otf)_9{\cdot}10CH_3CN$ (PM = 5799), $C_{203}H_{123}Gd_7N_{37}F_{27}O_{51}S_9$: C, 42.04; H, 2.12; N, 8.93. Found: C, 41.70; H, 2.26; N, 9.02.

**$[Tb\subset(TbL_2)_6](Otf)_9$ (8).** Anal. Calcd for $[Tb\subset(TbL_2)_6](Otf)_9{\cdot}10CH_3CN$ (PM = 5811), $Tb_7C_{203}H_{123}N_{37}F_{27}O_{51}S_9$: C, 41.95; H, 2.12; N, 8.93; S, 4.95. Found: C, 41.75; H, 2.22; N, 9.23; S, 5.15. ES$^+$-MS: *m*/*z* 1571.6 $\{[TbL_2]_6(Otf)_3\}^{3+}$, 1141.4 $\{[TbL_2]_6(Otf)_2\}^{4+}$.

**$[Eu\subset(GdL_2)_6](Otf)_9{\cdot}10CH_3CN$ (9).** Anhydrous $Eu(Otf)_3$ (12.0 mg, 0.020 mmol) was added to a suspension of $[GdL_2](Otf)$ (122 mg, 0.142 mmol) in acetonitrile (10 mL). The solution was stirred

(43) Jameson, D. L.; Guise, L. E. *Tetrahedron Lett.* **1991**, *32*, 1999−2002.

for 15 min until dissolution of the solid. The resulting solution was filtered, and diisopropylether was immediately added in sufficient amount to produce $[Eu\subset(GdL_2)_6](Otf)_9$ as a white solid (60 mg, 41% yield). Anal. Calcd for $[Eu\subset(GdL_2)_6](Otf)_9\cdot 10CH_3CN$ (PM = 6146.4), $C_{221}H_{150}EuGd_6N_{46}F_{27}O_{51}S_9$: C, 43.18; H, 2.45; N, 10.48; Eu, 2.34; Gd, 15.55. Found: C, 42.96; H, 2.40; N, 10.34; Eu, 2.47; Gd, 15.35.

**$[Lu\subset(EuL_2)_6](Otf)_9$ (10).** Anhydrous $Lu(Otf)_3$ (12.1 mg, 0.019 mmol) was added to a suspension of $[EuL_2](Otf)$ (100 mg, 0.117 mmol) in acetonitrile (15 mL). The solution was stirred and heated at ~70 °C for 30 min until dissolution of the solid. The resulting solution was filtered, and diisopropylether was added to produce $[Lu\subset(EuL_2)_6](Otf)_9$ as a white solid (70 mg, 58% yield). Single crystals suitable for diffraction analysis were grown by slow vapor diffusion of $Et_2O$ into a $2 \times 10^{-2}$ M MeCN solution of the complex. Anal. Calcd for $[Lu\subset(EuL_2)_6](Otf)_9\cdot 10CH_3CN$ (PM = 6137.6), $C_{221}H_{150}LuEu_6N_{46}F_{27}O_{51}S_9$: C, 43.18; H, 2.45; N, 10.48; Eu, 14.85. Found: C, 42.96; H, 2.40; N, 10.34; Eu, 14.61.

The proton NMR spectrum of the complex $[Lu\subset(EuL_2)_6](Otf)_9$ in acetonitrile was fully assigned by NOESY and COSY experiments and by comparison with the homopolymetallic europium complex (Figure 4).

**$[Tb\subset(EuL_2)_6](Otf)_9$ (11).** Anhydrous $Tb(Otf)_3$ (10.7 mg, 0.017 mmol) was added to a suspension of $[EuL_2](Otf)$ (91 mg, 0.106 mmol) in acetonitrile (15 mL). The solution was stirred for 30 min until dissolution of the solid. The resulting solution was filtered and diisopropylether was added to produce $[Tb\subset(EuL_2)_6](Otf)_9$ as a white solid (55 mg, 55% yield). Anal. Calcd for $[Tb\subset(EuL_2)_6](Otf)_9\cdot 3CH_3CN\cdot Et_2O$ (PM = 5925.07), $C_{211}H_{139}TbEu_6N_{39}F_{27}O_{52}S_9$: C, 42.77; H, 2.34; N, 9.21; Tb 2.68. Found: C, 42.66; H, 2.37; N, 8.96; Tb, 2.79.

The paramagnetism of the Tb and Nd ions prevented the assignment of the $^1H$ NMR spectra including these ions.

**Spectroscopic and Analytical Measurements.** $^1H$ NMR spectra were recorded on Bruker AM-200 and Varian U-400 spectrometers in $CD_3CN$ with $CH_3CN$ as the internal standard. Elemental analyses of the complexes were performed under argon by Analytische Laboratorien GmbH at Lindlar, Germany, and by the Service Central d'Analyses (Vernaison, France).

Absorption spectra were recorded on Cary 50 Probe UV−vis spectrometer with Perkin-Elmer luminescence cells with a path length of 1 cm. Solution luminescence lifetime measurements were recorded on a Perkin-Elmer LS-50B spectrometer at 293 K (without external temperature regulation). The phosphorescence lifetime ($\tau_L$) was measured by recording the decay at the maximum of the emission spectra. The signals were analyzed as single-exponential decays. The instrument settings were as follows: a gate time of 10 ms, an integration time of 1 s, a flash count of 5, excitation and emission slit widths of 2.5 nm, and a varied delay time. Lifetimes are the average of three independent experiments. Phosphorescence excitation and emission spectra were recorded on the same instrument with a delay of 0.00 ms, a gate time of 10 ms, a cycle time of 200 ms, and a flash count of 1. Solutions ($2 \times 10^{-4}$ M) of $[EuL_2](Otf)$, $[Eu\subset(EuL_2)_6](Otf)_9$, $[Lu\subset(EuL_2)_6](Otf)_9$, and $[Tb\subset(EuL_2)_6](Otf)_9$, for quantum yield measurements, were prepared by dissolution of the isolated complexes in acetonitrile or in situ by mixing of the appropriate volumes of $Ln(Otf)_3$ and $[EuL_2](Otf)$. Quantum yields, $\Phi$, have been calculated using the equation $\Phi_x/\Phi_r = A_r(\lambda)n_x^2D_x/A_s(\lambda)n_r^2D_r$, where $x$ refers to the sample, r refers to the reference, $A$ is the absorbance at the excitation wavelength, $n$ is the refractive index, and $D$ is the integrated emitted intensity. The tris(dipicolinate) complex $[Eu(dpa)_3^{3-}]$ ($H_2dpa$ = dipicolinic acid) ($\Phi$ = 24%, $7.5 \times 10^{-5}$ M in Tris buffer 0.1 M) and the $[Eu(tpaen)]^-$ (*N*,*N*,*N*′*N*′-tetrakis[(6-carboxypyridin-2-yl)methyl]-ethylenediamine = $H_4tpaen$) complex ($\Phi$ = 7%, $7.5 \times 10^{-5}$ M in Tris buffer 0.1 M) were used as references for the determination of quantum yields.[44,45]

A description of the equipment and experimental procedures for luminescence measurements in the visible range has been published previously.[46] Excitation of the finely powdered samples was achieved by a 450 W xenon high-pressure lamp coupled with a monochromator or a Coherent Innova argon laser, and the emission spectra were corrected for the instrumental function. Luminescent lifetimes were measured using excitation provided by a Quantum Brillant Nd:YAG laser equipped with frequency doubler, tripler, and quadrupler, as well as with an OPOTEK MagicPrism OPO crystal. The output signal of the photomultiplier was fed into a Stanford Research SR-430 multichannel scaler and transferred to a PC. Lifetimes are averages of 3 independent determinations. Quantum yields in the solid state were determined by an absolute method using an integration sphere coupled to a Spex Fluorolog FL-3-22 fluorimeter.[47]

**X-ray Crystallography.** All diffraction data were taken using a Bruker SMART CCD area detector three-circle diffractometer (Mo Kα radiation, graphite monochromator, $\lambda$ = 0.71073 Å). To prevent hydrolysis and reduce solvent loss, the crystals were coated with a light hydrocarbon oil and quickly transferred into a stream of cold nitrogen on the diffractometer.

The cell parameters were obtained with intensities detected on three batches of 15 frames. The crystal−detector distance was 5 cm. For three settings of $\Phi$ and $2\Theta$, narrow data frames were collected with 0.3° increments in $\omega$. A hemisphere of data was collected for **6**, and a quadrant of data was collected for **10**. Two hundred seventy images were collected for **7**. At the end of the data collection, the first 50 frames were recollected to establish that crystal decay had not taken place during the collection. Unique intensities with $I > 10\sigma(I)$ detected on all frames using the Bruker SMART program[48] were used to refine the values of the cell parameters. The substantial redundancy in data allows empirical absorption corrections to be applied using multiple measurements of equivalent reflections with the SADABS Bruker program.[48] Space groups were determined from systematic absences, and they were confirmed by the successful solution of the structure. Attempts were made to solve the structure in a noncentrosymmetric group ($P_1$, $P6_3$) which did not lead to a satisfactory result (impossibility of refining some atoms, most atoms with non-positive definite thermal parameters). The crystallographic data and selected bond distances for **6**, **7**, and **10** are listed in Tables 1 and 2, respectively. Complete information on crystal data, data collection parameters, and refinement details are given in the Supporting Information.

The structures were solved by direct methods using the SHELX-TL 6.10 package,[49] and all atoms in the hexameric cations were found by difference Fourier syntheses. The three structures consist of hexameric clusters encapsulating a central lanthanide ion. The presence of seven trivalent lanthanides in the cyclic clusters results in an overall cation charge of +9 which requires the presence of 9

(44) Chatterton, N.; Bretonnière, Y.; Mazzanti, M.; Pécaut, J. *Angew. Chem., Int. Ed.* **2005**, *44*, 7595−7598.
(45) Chauvin, A.-S.; Gumy, F.; Imbert, D.; Bünzli, J.-C. *Spectrosc. Lett.* **2004**, *37*, 517−532.
(46) Comby, S.; Imbert, D.; Chauvin, A.-S.; Bünzli, J.-C. *Inorg. Chem.* **2006**, *45*, 732−743.
(47) De, Mello, J. C.; Wittmann, H. F.; Friend, R. H. *Adv. Mater.* **1997**, *9*, 230.
(48) *SMART*; Bruker: Madison, WI, 1995.
(49) Sheldrick, G. M. *SADABS*, 6.14 ed.; University of Göttingen: Götttingen, Germany, 2000.

**Table 1.** Crystallographic Data for the Structures of Complexes **6**, **7**, and **10**

| | $[Nd\subset(NdL_2)_6](Otf)_9$ **6** | $[Gd\subset(GdL_2)_6](Otf)_9$ **7** | $[Lu\subset(EuL_2)_6](Otf)_9$ **10** |
|---|---|---|---|
| formula | $C_{211}H_{135}F_{27}N_{41}Nd_7O_5S_9$ | $C_{221}H_{150}F_{27}Gd_7N_{46}O_{51}S_9$ | $C_{218}H_{156}Eu_6F_{27}LuN_{42}O_{55}S_9$ |
| fw | 5871.82 | 6168.16 | 6132.12 |
| cryst syst | hexagonal | hexagonal | hexagonal |
| space group | $P6_3/m$ | $P6_3/m$ | $P6_3/m$ |
| $a$ (Å) | 22.417(3) | 22.996(7) | 22.368(4) |
| $b$ (Å) | 22.417(3) | 22.996(7) | 22.368(4) |
| $c$ (Å) | 30.021(7) | 31.319(2) | 30.07(1) |
| $V$ (Å$^3$)/$Z$ | 13065(4)/2 | 14342(1)/2 | 13031(6)/2 |
| $\lambda$ | 0.71073 | 0.71073 | 0.71073 |
| $D_{calcd}$ (g cm$^{-3}$) | 1.493 | 1.428 | 1.563 |
| $\mu$(Mo K$\alpha$) (mm$^{-1}$) | 1.532 | 1.750 | 1.968 |
| temp (K) | 193(2) | 223(2) | 193(2) |
| R1, wR2[a] | 0.1246, 0.2751 | 0.0695, 0.1947 | 0.0748, 0.1757 |

[a] Structure was refined on $F_0^2$ using all data: wR2 = $[\sum[w(F_0^2 - F_c^2)^2]/\sum w(F_0^2)^2]^{1/2}$, where $w^{-1} = [\sum(F_0^2) + (aP)^2 + bP]$ and $P = [\max(F_0^2, 0) + 2F_c^2]/3$.

**Table 2.** Selected Bond Distances (Å) in Complexes **5, 6,** and **7**[a]

| | $Eu_6Eu$ **5** | $Nd_6Nd$ **6** | $Gd_6Gd$ **7** |
|---|---|---|---|
| Ln(2)−O(1) | 2.272(6) | 2.297(6) | 2.268 (7) |
| Ln(1)−O(3)# | 2.387(6) | 2.437(5) | 2.385(7) |
| Ln(1)−O(4) | 2.394(6) | 2.404(5) | 2.354(6) |
| Ln(1)−O(2) | 2.420(6) | 2.437(5) | 2.432(6) |
| Ln(1)−N(6) | 2.502(8) | 2.575(7) | 2.498 (8) |
| Ln(1)−N(1) | 2.529(7) | 2.511(7) | 2.559(8) |
| Ln(1)−N(2) | 2.576(7) | 2.610(5) | 2.592(7) |
| Ln(1)−N(5) | 2.603(7) | 2.611(6) | 2.616(8) |
| Ln(1)−N(3) | 2.604(7) | 2.663(6) | 2.590(7) |
| Ln(1)−N(4) | 2.646(7) | 2.736(6) | 2.641(9) |
| Ln(1)−Ln(2) | 6.248 | 6.216 | 6.254 |
| Ln(1)−Ln(1)# | 6.298 | 6.289 | 6.304 |

[a] Symmetry transformations used to generate equivalent atoms: # $x - y$, $x$, $-z + 1$.

triflates. (In the experimental conditions used for the synthesis of complexes **6**, **7**, and **10**, the only possible counterions are triflates.) Because of the quality of the crystals, the high disorder of the triflates and solvent molecules, and their location on symmetry elements, to obtain a satisfactory model of the triflates and solvents, it was necessary to impose distance restraints and include missing atoms of partially located triflates and solvents.

Hydrogen atoms for all complexes were included in calculated positions, and the thermal parameters were refined isotropically. All the non-hydrogen atoms of the cyclic cation were anisotropically refined on $F^2$. The final $R$ values ranges from 7 to 12%.

## Results and Discussion

**Assembly of Homopolymetallic Complexes.** The reaction of $Ln(Otf)_3$ with 2 equiv of HL (L = 2,2′:6′,2″-terpyridine-6-carboxylic acid) in the presence of triethylamine in methanol leads to the formation of the mononuclear eight-coordinate complex $[Ln(L)_2](Otf)$ (Ln = Eu, **1**; Gd, **2**; Tb, **3**; Nd, **4**).

The $^1$H NMR spectrum in acetonitrile of these sparingly soluble complexes performed under anhydrous conditions shows only the presence of rigid $C_2$-symmetric species in agreement with the retention in solution of a monometallic structure analogous to the solid-state structure previously reported for **1**.[25]

These complexes dissociate in water as indicated by the NMR spectrum of a $\sim 10^{-2}$ M aqueous solution which shows only the presence of the free ligand.

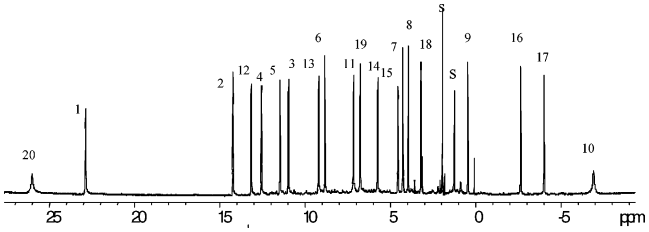


**Figure 1.** $^1$H NMR spectrum of a solution of $[Eu\subset(EuL_2)_6](Otf)_9$, **5**, in anhydrous $CD_3CN$ at 298 K and 400 MHz.

The addition of an excess of metal triflate (0.16−0.25 equiv) to a suspension of the sparingly soluble monometallic species in acetonitrile results in the complete dissolution of the $[LnL_2]Otf$ complexes and leads to the isolation of the isostructural polymetallic complexes $[Ln\subset(LnL_2)_6](Otf)_9$ (Ln = Eu, **5**; Nd, **6**; Gd, **7**; Tb, **8**). The X-ray crystallographic analysis of **5**−**7** reveals the presence of heptametallic complexes with a unique ring structure hosting a $Ln^{III}$ cation in its center. Because of the rapid solvent loss of the crystals of complex **8**, X-ray diffraction data were not of sufficient quality to report bond distances and angles, but the unit cell parameters and atom connectivity confirmed the isostructural nature of isolated complex. Satisfactory elemental analyses were also obtained for all complexes. The presence of the hexameric wheel in acetonitrile solution was confirmed by NMR and ESI-MS spectroscopy. The proton NMR spectrum of complex **5** in anhydrous acetonitrile (Figure 1) shows the presence of only one set of 20 signals in agreement with the presence of two terpyridinecarboxylate ligands in two different coordination environments. These features indicate that the complex retains the highly symmetric solid-state structure in solution. EXSY experiments carried out at different temperatures did not show any evidence of fast exchange processes in the temperature range of 243−343 K indicating high solution rigidity. The proton NMR spectrum shows that the dissolution of complex **5** in methanol leads to disruption of the cyclic structure to give the corresponding monometallic complexes.

The proton NMR spectrum of solutions of the $Nd^{III}$ complex **6** (Figure 2) shows the presence of one set of 20 signals as previously found for the europium complex. Additional low-intensity signals are also present in the spectrum, in agreement with the presence in solution of minor

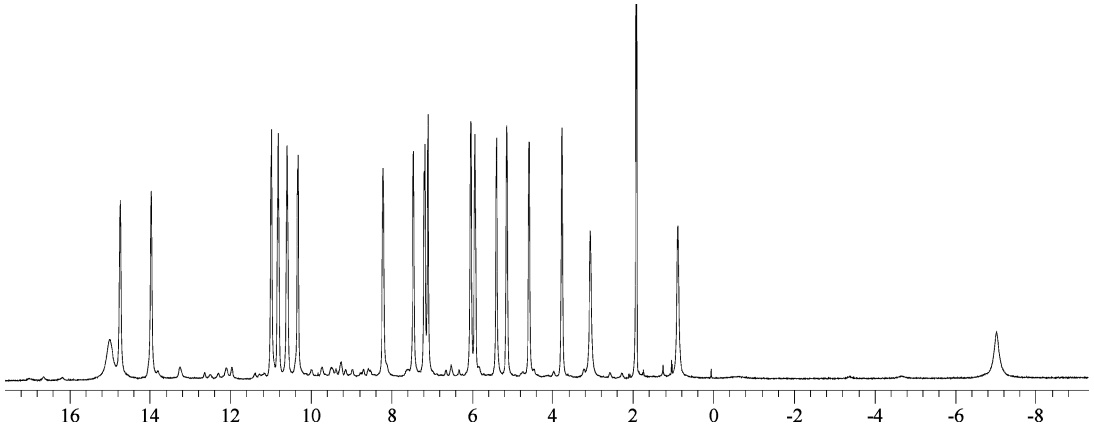


**Figure 2.** $^1$H NMR spectrum of $[Nd\subset(NdL_2)_6](Otf)_9$, **6**, in anhydrous $CD_3CN$ at 308 K and 400 MHz.

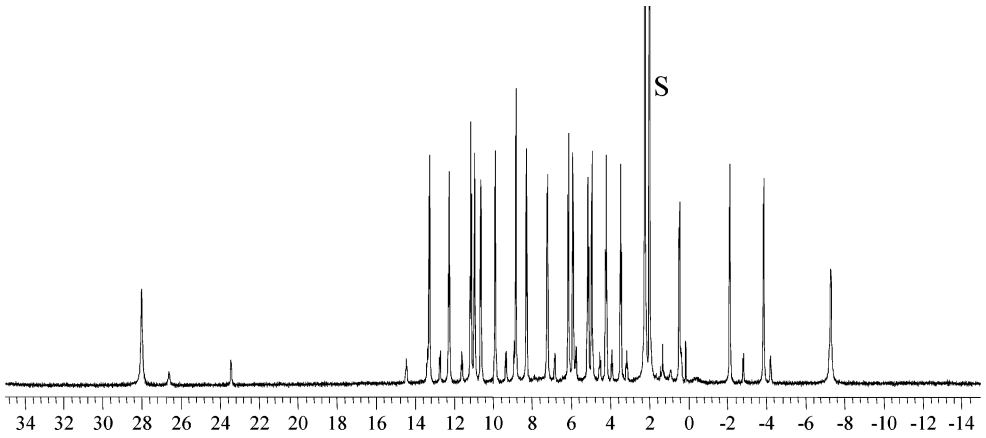


**Figure 3.** $^1$H NMR spectrum of a 6:1 mixture of $[EuL_2](Otf)$ and $Lu(Otf)_3$ in hydrous $CD_3CN$ (298 K, 400 MHz) after 24 h.

unidentified species. However, the formation of only one type of crystals corresponding to the heptametallic complex was observed in the solid state, as shown by elemental analysis and X-ray diffraction. For the lanthanum ion, dissolution of the monometallic species in acetonitrile consecutive to the addition of an excess of $La(Otf)_3$ (0.16 equiv) did not result in the formation of rigid solution species, but only broad peaks are observed in the NMR spectrum. The species formed were not further characterized. These results indicate that the nuclearity of the polymetallic complexes is controlled by the ionic radius of the central ion leading to the exclusive formation of hexameric rings for $Eu^{III}$, $Gd^{III}$, and $Tb^{III}$ ions. The presence of additional minor species for $Nd^{III}$ is most likely the consequence of its larger size which can allow the formation of species of different nuclearity. For the larger $La^{III}$ ion, the latter probably become prominent and are in rapid exchange on the NMR time scale.

The addition of an excess of metal triflate (0.16−0.5 equiv) to a suspension of $[LnL_2](Otf)$ in acetonitrile did not result in the formation of polymetallic species for the smaller lanthanide ions $Y^{III}$, $Yb^{III}$, or $Lu^{III}$.

These results show the template effect of the central cation in the assembly of the cyclic polymetallic structure and indicate that the self-assembly is controlled by the size of the lanthanide ion. The formation of the lanthanide wheel requires the presence of an accessible free coordination site on the eight-coordinated monometallic complex to allow the coordination of the bridging carboxylate. The smaller ionic radii of yttrium and lutetium do not permit the formation of carboxylate bridges, thus preventing the self-assembly process to occur.

**Assembly of Heteropolymetallic Complexes.** The molecular structure of the $[Ln\subset(LnL_2)_6](Otf)_9$ complexes presents two very different coordination environments and therefore is well adapted for the assembly of heterobimetallic complexes. We have therefore investigated the possibility of developing a synthetic strategy to assemble pure heteropolymetallic complexes.

Proton NMR studies in hydrous acetonitrile show that the addition of 0.16 equiv of $[Ln(Otf)_3]$ for Ln = Ho−Lu (ions with smaller ionic radii than Eu) to a suspension of the monometallic species $[EuL_2](Otf)$ leads to the formation of the homopolymetallic complex $[Eu\subset(EuL_2)_6](Otf)_9$ and of only one additional heteropolymetallic species (Figure 3). The $^1$H proton spectra of these heterometallic species are highly symmetric with only 20 signals for the 12 terpyridine-2-carboxylate ligands in agreement with the presence of the complexes $[Ln\subset(EuL_2)_6](Otf)_9$ in which the smaller Ln ion is located in the center of the cyclic framework. Indeed, the distribution of the second metal ion on the periphery of the cyclic structure would result in asymmetric solution species giving rise to a larger number of $^1$H NMR signals. The addition of larger amounts of $Lu(Otf)_3$ (0.25−1 equiv) to the monometallic europium complex, followed by heating of the reaction mixture results in the complete conversion

of the homometallic europium complex into the heterometallic $[Lu\subset(EuL_2)_6](Otf)_9$ associated with the formation of $[LuL_2](Otf)$. An X-ray diffraction study confirmed the presence of the heteropolymetallic complex $[Lu\subset(EuL_2)_6](Otf)_9\cdot 6CH_3CN\cdot 2H_2O\cdot Et_2O\cdot MeOH$, **10**.

The addition of 0.16 equiv of $Ln(Otf)_3$ for Ln = La, Sm, and Tb (ions with ionic radii larger than $Eu^{III}$ or very similar to $Eu^{III}$) to a suspension of the monometallic species $[EuL_2](Otf)$ leads to mixtures of species displaying a very complicated NMR spectrum.

These results indicate that the tetradentate ligand 2,2′:6′,2″-terpyridine-6-carboxylate allows the selective production of heteropolymetallic complexes when the peripheral ions are significantly larger than the central ion.

In anhydrous acetonitrile, the reaction of $Sm(Otf)_3$ with $[EuL_2](Otf)$ in a 1:6 ratio results in the immediate selective self-assembly of one major symmetric species. However the proton NMR spectrum changes after 48 h leading to an approximately 1:1 mixture of the symmetric species $[Sm\subset(EuL_2)_6](Otf)_9$ and an asymmetric species of probable general formula $[Eu\subset(SmL_2)_1(EuL_2)_5](Otf)_9$. After three weeks, the $^1H$ spectrum has dramatically evolved and shows the presence of a complicated mixture of species similar to what was observed under hydrous conditions (Figure S1, Supporting Information). We were not able to see exchange between the different species by EXSY experiments for the samarium reaction mixture, suggesting that the different solution species are rigid. For photophysical study purposes, we investigated the possibility of isolating the heterometallic complex $[Eu\subset(GdL_2)_6](Otf)_9$ (**9**), which presents a slightly larger cation on the central site. The immediate addition of isopropylether, after reaction of $Eu(Otf)_3$ with the monometallic species $[GdL_2](Otf)$ in stoichiometric ratio of 1:6 allowed the isolation of $[Eu\subset(GdL_2)_6](Otf)_9$, (**9**) for which satisfactory analytical data were obtained.

In rigorously anhydrous acetonitrile, the reaction of $Ln(Otf)_3$ for Ln = Tb, Er, Yb, and Lu with the monometallic species $[EuL_2]Otf$ leads to the highly selective self-assembly of the heterobimetallic species $[Ln\subset(EuL_2)_6](Otf)_9$ (Ln = Tb, Er, Yb, Lu) as indicated by the NMR spectra which show the presence of only one $C_6$-symmetric species. Complexes $[Lu\subset(EuL_2)_6](Otf)_9$ (**10**) and $[Tb\subset(EuL_2)_6](Otf)_9$ (**11**) were isolated in a similar way and characterized. The X-ray diffraction study of complex **11** shows that the complex is isostructural with the homopolymetallic compounds **6**, **7**, and **8**, but the quality of the crystals and the similarity of the two ions make it difficult to unambiguously locate the two different cations. The elemental analyses of the isolated compounds are in agreement with the presence of species presenting a 1:6 Ln′/Eu ratio. The proton NMR spectrum of **10** (Figure 4) is in agreement with a highly symmetric solution structure in which the two metals remain bound to the terpyridinecarboxylate ligands on the NMR time scale and did not indicate any rearrangement involving metal scrambling over long periods of time (up to 24 months). EXSY experiments carried out at different temperatures did not show any evidence of fast exchange processes in the temperature range of 243−343 K suggesting that the metals remain coordinated to the ligand even at high temperature.

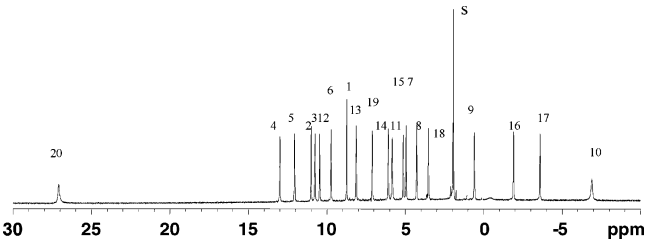


**Figure 4.** $^1H$ NMR spectrum of $[Lu\subset(EuL_2)_6](Otf)_9$ in anhydrous $CD_3CN$ at 298 K and 400 MHz.

The $^1HNMR$ spectra of complexes **5** and **10** are very similar suggesting an analogous solution structure for the two complexes. Only the signals assigned to the pyridine protons next to the carboxylate binding the central atom are significantly affected by the replacement of the paramagnetic $Eu^{III}$ ion with the diamagnetic $Lu^{III}$ ion. The $^1H$ NMR spectrum of complex **11** (Figure 5) also shows the presence of highly symmetric solution species with only 20 signals for the 12 terpyridine-2-carboxylate ligands. The more important differences observed for the spectrum including a terbium ion with respect to the homometallic europium complex (signals are spread over a larger spectral window) arise probably only from the high paramagnetic character of the $Tb^{III}$ ion. However, the $^1H$ NMR spectrum of the complex **11** evolves with time, and after a week, the signals assigned to the homopolymetallic europium wheel appear (in ∼10% ratio), showing that rearrangement can occur for the $[Tb\subset(EuL_2)_6](Otf)_9$ complex. This evolution is in agreement with the similar thermodynamic stability expected for these species because of the high similarity of the Tb and Eu ions. No evolution was observed over a week period for the heteropolymetallic complexes $[Ln\subset(EuL_2)_6](Otf)_9$ for Ln = Er and Yb prepared in situ.

These results indicate that the selective formation of heteropolymetallic complexes is controlled by the cation sizes. Smaller lanthanides prefer the central site, while larger ions favor the peripheral sites. In the peripheral sites, $Ln^{III}$ ions are nine-coordinated by three oxygen donors and six nitrogen atoms, while in the central site, the ions are coordinated by six oxygen donors. The inclusion of the smaller lanthanide ions in the central site is favored both by their smaller size (lower coordination number) and by their higher Lewis acid character favoring oxygen donors over nitrogen donors. In anhydrous conditions, heterometallic species are selectively obtained, while in the presence of water, formation of the homopolymetallic complex is also observed probably because of the much higher concentration of noncomplexed $Eu^{3+}$ in these conditions.

The addition of a larger ion to the $[EuL_2](Otf)$ complex in anhydrous acetonitrile leads also to the immediate formation of the kinetically favored $[Sm\subset(EuL_2)_6](Otf)_9$ as the major species. However, the complex slowly rearranges over a period of a few weeks yielding a complex mixture of species. In the presence of water, which causes the partial dissociation of the $[EuL_2](Otf)$ complex, the formation of a mixture of species is more rapid.

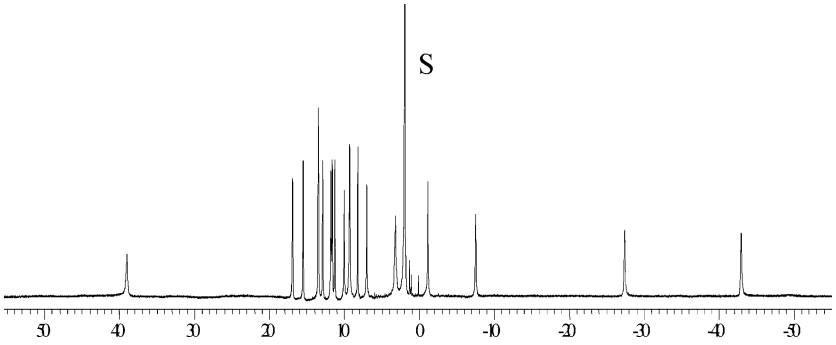


**Figure 5.** $^1$H NMR spectrum of $[Tb\subset(EuL_2)_6](Otf)_9$ in anhydrous $CD_3CN$ at 298 K and 400 MHz.

For ions only slightly smaller than europium (such as Tb), the kinetically favored complex $[Tb\subset(EuL_2)_6](Otf)_9$ forms at first in both anhydrous and hydrous conditions. In presence of traces of water, some metal scrambling is observed, but $[Tb\subset(EuL_2)_6](Otf)_9$ can be isolated from anhydrous acetonitrile solutions. These results suggest that self-assembly of the heteropolymetallic species $[Ln\subset(EuL_2)_6](Otf)_9$ with Ln significantly smaller (Er−Lu) than $Eu^{III}$ is under thermodynamic control. The formation of similar sets of heteropolymetallic complexes presenting Nd, Sm, Gd, or Tb in the peripheral sites can be anticipated.

**Crystal and Molecular Structure of Homo- and Heteropolymetallic Wheels.** The homopolymetallic complexes $[Eu(2)\subset(Eu(1)L_2)_6](Otf)_9\cdot10CH_3CN$ (**5**)[25], $[Nd(2)\subset(Nd(1)L_2)_6](Otf)_9\cdot5CH_3CN$ (**6**), and $[Gd(2)\subset(Gd(1)L_2)_6](Otf)_9\cdot10CH_3CN$ (**7**) are isostructural. Selected interatomic distances are given in Table 2. The crystal structures of complexes **5**, **6**, and **7** consist of discrete $[Ln(2)\subset(Ln(1)L_2)_6]^{9+}$ ions, uncoordinated disordered triflate ions, and disordered solvent molecules. The molecular structure of the $[Ln(2)\subset(Ln(1)L_2)_6]^{9+}$ cations confirms the formation of an hexameric wheel encapsulating a lanthanide ion in its center for the three cations. A $S_6$ crystallographic axis passes through the center. The six nine-coordinated $[Ln(1)L_2]$ moieties are connected by six bridging carboxylates forming a ring. The coordination polyhedron of Ln(1) is best described as a distorted monocapped square antiprism for the $Eu^{III}$ and $Gd^{III}$ complexes. A more important distortion is observed for the $Nd^{III}$ complex. The angles between the mean planes of the two coordinated terpyridine unit vary from 56.4 ($Nd^{III}$) to 77.8 ($Eu^{III}$) and 77.1° ($Gd^{III}$). The mean Eu(1)−O distance (2.40(2) Å) is significantly longer than the corresponding distance found in **1** (2.31(1) Å). The Ln(1)−O(4) and Ln(1)−O(3) distances are very similar for the three ions despite the differences in ionic radii ($\Delta r_i$ between $Nd^{III}$ and $Gd^{III}$ = 0.056 Å).[50] The Ln(1)−O(3) distances are almost identical for $Gd^{III}$ and $Eu^{III}$ in agreement with the small difference in their ionic radii ($\Delta r_i$ = 0.013 Å). Conversely, the difference between the Nd(1)−O(3) and Gd(1)−O(3) distances (0.052 Å) is larger ($\Delta r_i$ = 0.058 Å). The Ln(2) cation located in the ring center presents a regular octahedral coordination geometry. The Ln(2)−O distances are almost identical for $Eu^{III}$ and $Gd^{III}$ (2.27(1) Å). The decrease in the Ln(2)−O distance between $Nd^{III}$ and $Eu^{III}$ (0.025 Å) is significantly smaller than the difference in ionic radii. This is the consequence of the nuclearity of the polymetallic structure. Longer Ln(2)−O distances would result in longer Ln(1)−O(3) (bridging carboxylate), rendering the architecture less stable. This is in agreement with a lower stability of the hexametallic ring for larger ions and with the observation of minor species in solution for neodymium. In spite of the lengthening of all the Ln−O and Ln−N distances observed in the $Nd^{III}$ wheel with respect to the $Eu^{III}$ and $Gd^{III}$ ones, a significant decrease is found for the Ln(1)−Ln(2) and the Ln(1)−Ln(1) distances leading to a overall smaller ring for the larger ions. This can be rationalized in terms of the wider Ln(2)−Ln(1)−O(2) and Ln(1)−Ln(2)−O(1) angles observed in the $Nd^{III}$ complex (2.23 and 33.52°) with respect to $Eu^{III}$ (0.69 and 31.87°) and $Gd^{III}$ (0.99 and 32.14°). The six crystallographically equivalent lanthanide ions of the centrosymmetric cation $[Ln(2)\subset(Ln(1)L_2)_6]^{9+}$ are located in the corners of a pseudohexagon with a diameter (defined as the distance of two opposite $Ln^{III}$ ions) of 12.43 Å for Nd $^{III}$ and 12.50 Å for $Eu^{III}$ and $Gd^{III}$ (Figure 6). The pseudohexagon deviates only slightly from planarity with three Ln(1) ions situated above and three Ln(1) ions situated below (±0.46 Å in **5**, ±0.47 Å in **6**, and ±0.45 Å in **7**) the mean plane passing through the central Ln(2). The six carboxylate O(2) atoms are also located in the corners of a pseudohexagon with a smaller deviation from planarity (±0.32 Å in **5**, ±0.38 Å in **6**, and ±0.28 Å in **7**).

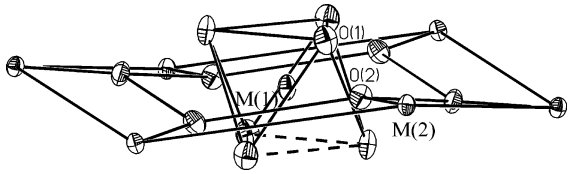


**Figure 6.** Side view of the coordination polyhedron of Ln(2) and of the hexagon formed by the carboxylate oxygens and by the six Ln(1) ions in the heptanuclear cations $[Ln(2)\subset(Ln(1)L_2)_6]^{9+}$.

The crystal structure of the heterometallic complex $[Lu\subset(EuL_2)_6](Otf)_9\cdot6CH_3CN\cdot2H_2O\cdot Et_2O\cdot MeOH$, **10**, is shown in Figure 7 (asymmetric unit in Figure 8), and selected interatomic distances are given in Table 3. The replacement of the central $Eu^{III}$ ion in the homopolymetallic complex **5** by a $Lu^{III}$ ion does not result in significant modification of the structure. The Eu(1)−N (2.58(5) Å) and Eu(1)−O (2.40(2) Å) mean distances remain unchanged with respect to the $[Eu\subset EuL_2)_6]^{9+}$ cation, while the Ln(2)−O distance decreases by 0.09 Å paralleling the decrease in ionic radii. The short Eu−Lu distance results in an overall decrease in the diameter

(50) Shannon, R. D. *Acta Crystallogr.* **1976**, *A32*, 751−767.

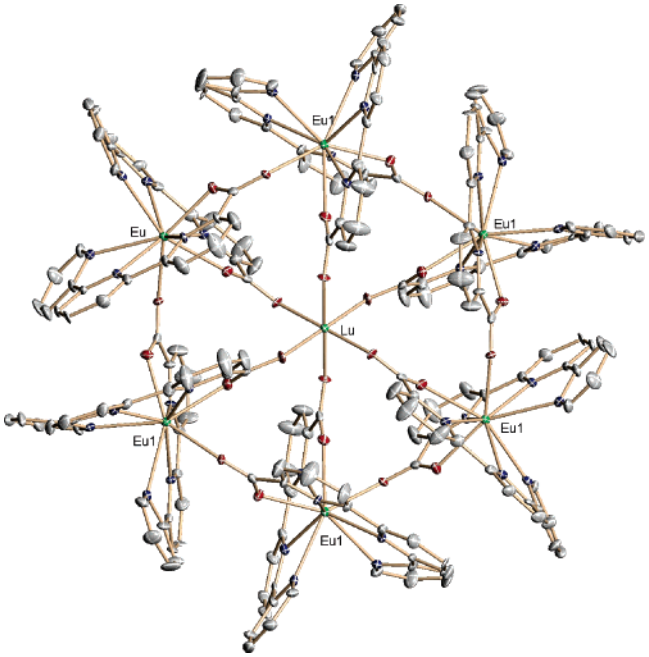


**Figure 7.** ORTEP view of the $[Lu\subset(EuL_2)_6]^{9+}$ cation in complex **10**, with thermal ellipsoids at the 30% probability level.

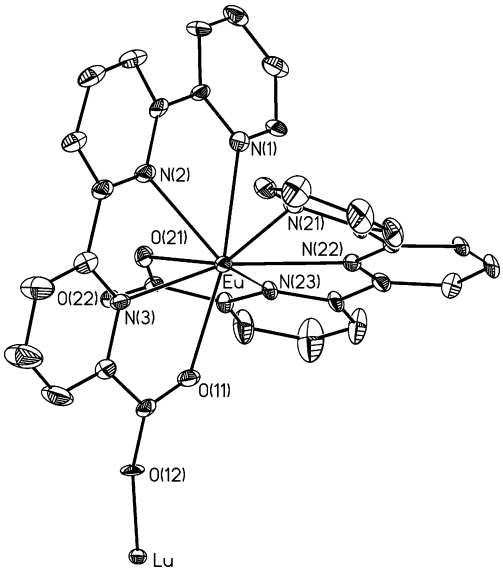


**Figure 8.** ORTEP view of the asymmetric unit of complex **10** with thermal ellipsoids at the 30% probability level.

of the europium ring (12.35 Å for the heterometallic complex versus 12.50 Å for the homopolymetallic) without producing significant structural variations (Lu−Eu−O(11) = 0.99°, Eu−Lu−O(12) = 32.10°; distance of the $Eu^{III}$ ions from the hexagon plane is ±0.45 Å). This suggests that the central site of the hexameric europium ring is well adapted to host small lanthanide ions, in agreement with the high solution rigidity of the heterometallic complexes.

**Metal-Centered Luminescence of [EuL$_2$](Otf).** A photophysical study of the precursor complex [EuL$_2$](Otf) has been performed to detect its presence in the spectra of the $[Eu\subset(EuL_2)_6](Otf)_9$ complex. The high-resolution excitation spectrum in the spectral range of the $^5D_0 \leftarrow {}^7F_0$ transition obtained by monitoring the maximum of the $^5D_0 \rightarrow {}^7F_2$ transition at low temperature displays a symmetrical peak at 17 211 cm$^{-1}$ with a full width at half-height (fwhh) of 9.2 cm$^{-1}$. Increasing the temperature to 295 K results in a typical shift of this line at 17 222 cm$^{-1}$ (fwhh = 9.8 cm$^{-1}$). The emission spectra display the characteristic Eu($^5D_0 \rightarrow {}^7F_j$) transitions (Figure S2, Supporting Information) and are dominated by the transitions to the $^7F_2$ sublevels. The electronic sublevels of the $^7F_j$ ($J$ = 1−4) manifold are reported above, in Table 4. Upon broadband excitation, the crystal field splitting of the emission spectra can be interpreted in terms of a low symmetry, $C_{2v}$. The $^5D_0 \rightarrow {}^7F_0$ transition is very weak. At 10 K, there are three main bands to the $^7F_1$ level, corresponding to $A_1 \rightarrow A_2$, $A_1 \rightarrow B_1$, and $A_1 \rightarrow B_1$ transitions, which are both allowed in $C_{2v}$ symmetry; the energy gaps between the levels are 90 and 99 cm$^{-1}$, respectively, while the total splitting is 189 cm$^{-1}$.

**Table 3.** Selected Bond Distances (Å) in Complex **10**[a]

| | |
|---|---|
| Lu−O(12) | 2.182(5) |
| Eu−O(22)# | 2.380(6) |
| Eu−O(21) | 2.385(5) |
| Eu−O(O11) | 2.424(6) |
| Eu−N(23) | 2.510(7) |
| Eu−N(1) | 2.634(6) |
| Eu−N(2) | 2.574(7) |
| Eu−N(22) | 2.574(7) |
| Eu−N(3) | 2.506(7) |
| Eu−N(21) | 2.703(7) |
| Eu−Lu | 6.177 |
| Eu−Eu# | 6.243 |

[a] Symmetry transformations used to generate equivalent atoms: # $y, -x + y, -z + 1$.

**Table 4.** Energy (cm$^{-1}$) of the Identified Crystal-Field Sublevels of the Eu($^7F_j$) Manifold ($J$ = 1−4) as Determined from Excitation and Emission Spectra in Solid State at 10 K[a]

| | [EuL$_2$](Otf) | | [Eu⊂(EuL$_2$)$_6$](Otf)$_9$ | | | |
|---|---|---|---|---|---|---|
| $\tilde{\nu}_{ex}$ (cm$^{-1}$) | 27 397 | 17 211 | 27 777 | | 17 181 | 17 221 |
| $^5D_0$ | 17 211 | 17 211 | 17 182 | 17 221 | 17 182 | 17 221 |
| $^7F_1$ | 296 | 289 | 325 | 286 | 317 | 280 |
| | 386 | 387 | 371 | 332 | 348 | 326 |
| | 485 | 487 | 416 | 377 | 413 | 518 |
| | | | 470 | 431 | | |
| | | | 512 | 473 | | |
| | | | 560 | 521 | | |
| $^7F_2$ | 963 | 960 | 963 | 924 | 892 | 918 |
| | 994 | 991 | 1010 | 971 | 947 | 969 |
| | 1050 | 1036 | 1037 | 998 | 995 | 1045 |
| | 1108 | 1051 | 1089 | 1050 | 1013 | 1095 |
| | | 1107 | 1139 | 1100 | 1078 | 1183 |
| | | | | | 1107 | |
| $^7F_3$ | 1915 | 1847 | 1878 | 1839 | 1852 | 1832 |
| | | 1913 | 1911 | 1872 | 1905 | 1867 |
| | | | 1934 | 1895 | | 1935 |
| | | | 1979 | 1940 | | 1970 |
| | | | 2014 | 1975 | | 2019 |
| | | | 2060 | 2021 | | |
| $^7F_4$ | 2694 | 2691 | 2647 | 2608 | 2821 | 2603 |
| | 2823 | 2821 | 2678 | 2639 | 2840 | 2718 |
| | 2839 | 2838 | 2759 | 2720 | 2873 | 2814 |
| | 2936 | 2861 | 2857 | 2818 | 2899 | 2841 |
| | | 2934 | 2882 | 2843 | 3041 | 2913 |
| | | 2942 | 2954 | 2915 | 3063 | 2948 |
| | | 2991 | 2991 | 2952 | | 3047 |
| | | 3026 | 3098 | 3059 | | 3057 |
| | | 3171 | 3134 | 3095 | | |

[a] $^5D_0$ is taken as the origin.

**Table 5.** Lifetimes of the Eu($^5D_0$) Excited Level (ms) in [$EuL_2$](Otf) and [$Ln\subset(LnL_2)_6$]$^{9+}$complexes in Solid State under Various Excitation Conditions at 10 and 295 K[a]

| compound | site | $T$ (K) | $\nu_{exc}$ ($cm^{-1}$) | $\tilde{\nu}_{an}$ ($cm^{-1}$) | $\tau$ (ms) |
|---|---|---|---|---|---|
| [$EuL_2$](Otf) | All | 10 | 28 169 | $^7F_2$ | 1.71(2) |
| | II | | 17 207 | $^7F_2$ | 1.60(1) |
| | All | 295 | 28 169 | $^7F_2$ | 1.51(2) |
| | II | | 17 217 | $^7F_2$ | 1.57(1) |
| [$Eu\subset(EuL_2)_6$](Otf)$_9$ | All | 10 | 28 169 | $^7F_2$ | 1.77(2) |
| | I | | 17 181 | $^7F_2$ | 2.02(1) |
| | III | | 17 219 | $^7F_2$ | 1.74(1) |
| | All | 295 | 28 169 | $^7F_2$ | 1.77(2) |
| | I | | 17 181 | $^7F_2$ | 1.71(2) |
| [$Tb\subset(EuL_2)_6$](Otf)$_9$ | All | 10 | 28 169 | $^7F_4$ | 1.73(1) |
| | I | | 17 182 | $^7F_1-^7F_2$ | 2.02(1) |
| | II | | 17 206 | $^7F_2-^7F_4$ | 1.68(1) |
| | III | | 17 218 | $^7F_1-^7F_2-^7F_4$ | 1.73(2) |
| | All | 295 | 28 169 | $^7F_2-^7F_4$ | 1.69(1) |
| | I | | 17 190 | $^7F_2-^7F_4$ | 1.65(1) |
| | II | | 17 217 | $^7F_2-^7F_4$ | 1.72(1) |
| [$Eu\subset(GdL_2)_6$](Otf)$_9$ | All | 10 | 28 169 | $^7F_2$ | 2.41(4) |
| | I | | 17 184 | $^7F_1-^7F_2$ | 1.90(1) |
| | II | | 17 208 | $^7F_2$ | 1.68(1) |
| | All | 295 | 28 169 | $^7F1-^7F_2$ | 2.10(1) |
| | I | | 17 192 | $^7F_2$ | 2.05(1) |
| [$Lu\subset(EuL_2)_6$](Otf)$_9$ | All | 10 | 28 169 | $^7F_2$ | 1.85(1) |
| | III | | 17 218 | $^7F_2$ | 1.92(11) |
| solution | All | | 28 169 | $^7F_2-^7F_4$ | 1.64(8) |
| solution | III | | 17 218 | $^7F_2$ | 1.68(1) |
| | All | 295 | 28 169 | $^7F_2$ | 1.91(5) |
| | III | | 17 224 | $^7F_2$ | 1.86(4) |
| solution | All | | 28 169 | $^7F_2-^7F_4$ | 2.22(3) |
| solution | III | | 17 224 | $^7F_2$ | 2.20(6) |

[a] Analyzing wavelength set on the maximum of the $^5D_0 \rightarrow {}^7F_{1,2,4}$, and $\sigma$ is given in parentheses.

The $^5D_0 \rightarrow {}^7F_2$ transition displays four bands close in energy, assigned to the allowed electric dipole transitions, $A_1 \rightarrow A_1$ and $A_1 \rightarrow B_1$, $B_2$ in $C_{2v}$ symmetry. The $^5D_0 \rightarrow {}^7F_4$ transition displays only three main components. Moreover, the emission spectrum upon selective excitation (17 211 $cm^{-1}$) is quite similar, except for the appearance of additional emission lines resulting from vibronic transitions (Figure S3, Supporting Information). There are three transitions to the $^7F_1$ level and four to the $^7F_2$ level. Analysis of the $^5D_0 \rightarrow {}^7F_4$ transition shows three main components at 14 530, 14 391 (splitting of 17 $cm^{-1}$), 14 282 (splitting of 8 $cm^{-1}$) and four weak ones at 14 359, 14 225, 14 190, and 14 053 $cm^{-1}$ (7 transitions are allowed in $C_{2v}$ symmetry). At 295 K, the emission spectrum becomes broader, as expected from a larger contribution from vibronic components.

The luminescence decay of the $^5D_0$(Eu) emission is a single-exponential function (Table 5) and corresponds to a 1.60 ms lifetime at 10 K, which is temperature-independent (1.57 ms at 295 K). These data confirm the absence of OH oscillators in the inner coordination sphere of the metal ion as demonstrated by the X-ray structure. Excitation through the $^1\pi\pi^*$ ligand state results in similar lifetimes, indicating a fast energy transfer from the ligand to the 4f states.

**Metal-Centered Luminescence of Polymetallic Complexes.** In the solid state, at both 295 and 10 K, the ligand-centered $^1\pi\pi^*$ emission is not detected, pointing to a quantitative L $\rightarrow$ $Eu^{III}$ energy-transfer process. The emission spectra display the characteristic Eu($^5D_0 \rightarrow {}^7F_j$) transitions

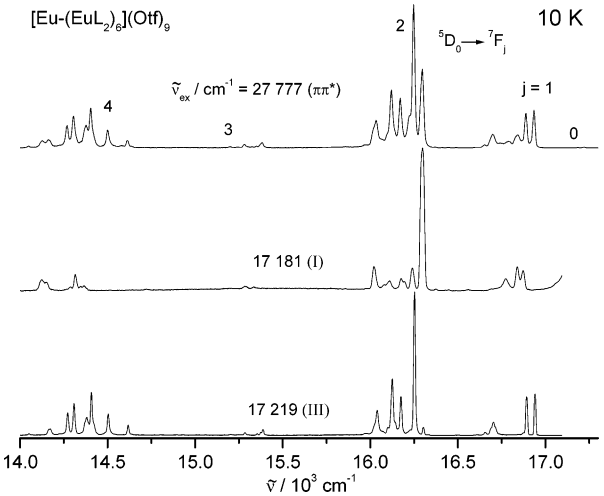


**Figure 9.** Emission spectra of the [$Eu\subset(EuL_2)_6$](Otf)$_9$ complex at 10 K upon broadband and selective excitation.

(Figure 9 and Figure S4, Supporting Information) and are dominated by the transitions to the $^7F_2$ sublevels. Energies of the electronic sublevels of the $^7F_j$ ($J = 1-4$) manifold are listed in Table 4. The weak $^5D_0 \rightarrow {}^7F_0$ transition, which is unique for a given chemical environment, occurs at 17 219 $cm^{-1}$. However, it also displays a faint component at 17 181 $cm^{-1}$ (site I). The $^5D_0 \rightarrow {}^7F_j$ transitions contain more components than expected. The spectrum displays weak bands arising from the emission of a second europium ion, indicating the presence of two different metal ion environments. A qualitative population analysis of the $^5D_0 \rightarrow {}^7F_0$ and $^5D_0 \rightarrow {}^7F_1$ transitions reveals the minor $Eu^{III}$ site, accounting for about 30%. The observation of two luminescent sites in [$Eu\subset(EuL_2)_6$](Otf)$_9$ is in good agreement with both the formulation and molecular structure of the investigated compound. However, the emission spectrum should reflect the presence of two different metal ion sites in a 6:1 ratio. The apparent contradiction can be explained by possible energy transfers from the major site, with a $^5D_0$ level at higher energy, to the central $Eu^{III}$, resulting in enhanced emission from the latter. To investigate further the emission of the central $Eu^{III}$ ion, we have resorted to high-resolution laser-excited excitation spectroscopy of the $^5D_0 \leftarrow {}^7F_0$ transition.

The excitation profile of the Eu($^5D_0 \leftarrow {}^7F_0$) transition obtained by monitoring all of the most intense components of the $^5D_0 \rightarrow {}^7F_2$ transition (large-band excitation spectrum) at 10 K (Figures 10 and 11) displays a main component at 17 219 $cm^{-1}$ and a weak one at 17 181 $cm^{-1}$, pointing to emission from two sites labeled III and I, respectively. The spectra obtained by monitoring individual components of the $^5D_0 \rightarrow {}^7F_2$ transition display both bands I and III, as well as an additional component labeled II (17 207 $cm^{-1}$). The latter is very faint and results from a small decomposition of the complex. An emission spectrum obtained upon exciting selectively this site is clearly different from the other spectra reported in Figure 10 but similar to the spectrum obtained for [$EuL_2$](Otf). From these data, a first conclusion is that the investigated compound contains two types of luminescent sites beside traces of [$EuL_2$](Otf): (i) a strongly emitting site III, arising from peripheral $Eu^{III}$ ions and (ii) site I,

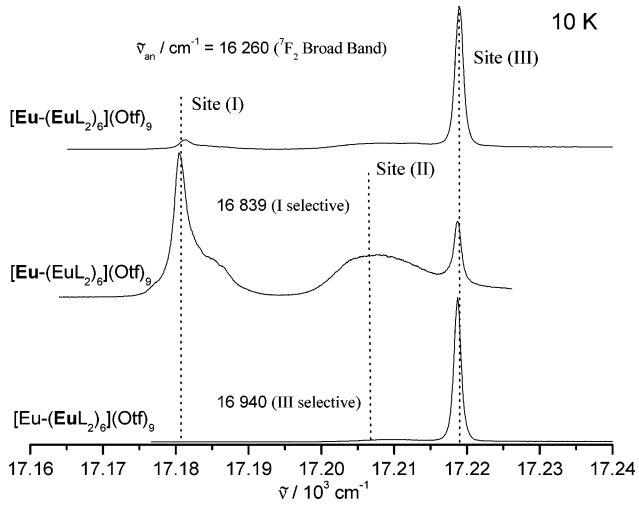


**Figure 10.** Excitation spectra at 10 K of the [Eu⊂(EuL$_2$)$_6$](Otf)$_9$ complex upon monitoring the Eu($^5D_0 \rightarrow {}^7F_{2,}$) transition (large band or selective analysis).

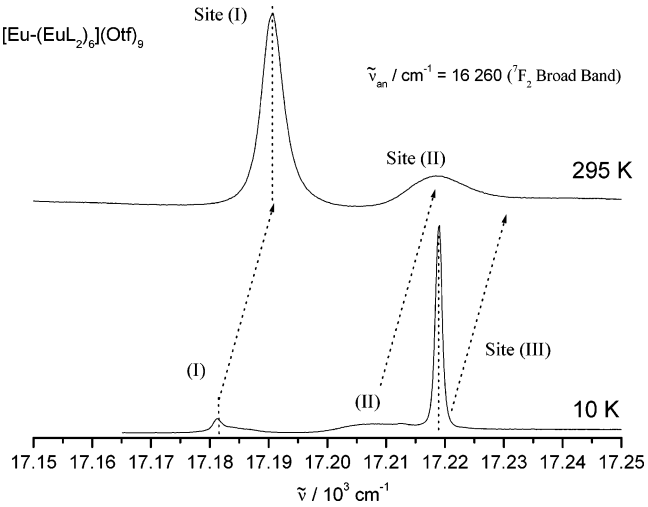


**Figure 11.** Broadband excitation spectra at 10 and 295 K of the [Eu⊂-(EuL$_2$)$_6$](Otf)$_9$ complex upon monitoring the Eu($^5D_0 \rightarrow {}^7F_{2,}$) transition.

corresponding to the central europium ion. Increasing the temperature up to 295 K (Figure 12) results in a typical shift of the lines at 17 191 and 17 219 cm$^{-1}$ for sites I and II, respectively. Surprisingly, the major species, site III completely disappears at room temperature, and the major emitting species becoming the central site I.

At low temperature, excitation at 17 219 cm$^{-1}$ (site III, Figure 9) yields an emission spectrum that can be analyzed in $C_2$ symmetry, although it contains more components than expected, again because of the presence of vibronic transitions. There are three main transitions not equally spaced to the $^7F_1$ level, corresponding to one A → A (16 703 cm$^{-1}$) and two A → B (16 941 and 16 895 cm$^{-1}$) transitions, which are both allowed in $C_2$ symmetry. The $^5D_0 \rightarrow {}^7F_2$ transition displays five bands assigned to the allowed three A → A and two A → B transitions. Analysis of the $^5D_0 \rightarrow {}^7F_4$ transition shows seven main components. In fact, the local $C_2$ symmetry probably arises from a distortion of a higher symmetry. In the crystal structure of the compound, the coordination polyhedron is indeed described as being a

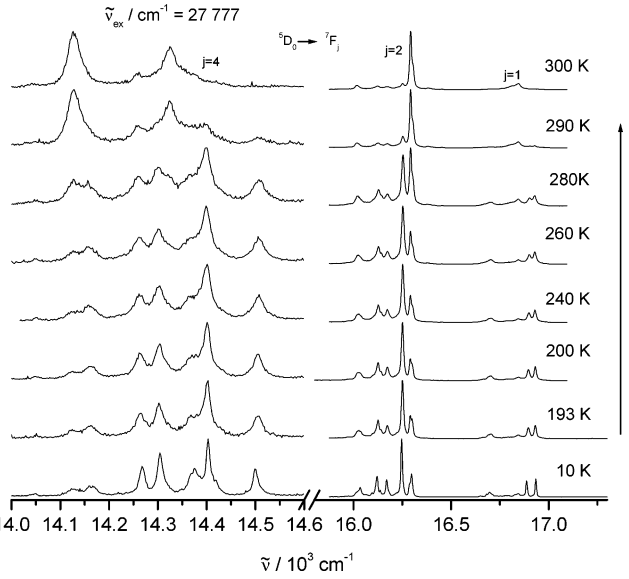


**Figure 12.** Emission spectra of the [Eu⊂(EuL$_2$)$_6$](Otf)$_9$ complex from 10 to 300 K upon broadband excitation.

distorted monocapped square antiprism. Excitation at 17 181 cm$^{-1}$ (site I, Figure 9) yields an unexpected emission spectrum: the crystal structure points to central Eu$^{III}$ ion lying on an inversion center ($O_h$), and in this case, all the electric dipole transitions are forbidden so that $^5D_0 \rightarrow {}^7F_1$ should be the most intense transition. In reality, the observed emission spectrum displays all the Eu($^5D_0 \rightarrow {}^7F_j$) transitions and is dominated by the $^5D_0 \rightarrow {}^7F_2$ transition. A possible explanation could be that the geometry of the excited-state reflected in the emission spectra is slightly different from the ground state geometry. However, a more probable explanation is that the crystal structure represents an average structure, with idealized symmetry, while the central Eu$^{III}$ ions in fact do not experience perfect octahedral geometry. The presence in the crystal of the same noncentrosymmetric species in different orientations can give rise to a pseudo inversion center and prevents the resolution of the structure in a crystallographic group of lower symmetry. And since Eu$^{III}$ emission spectra are highly sensitive to slight distortions from symmetry with an inversion center, we observe a spectrum corresponding to the absence of such a symmetry element.

Therefore, all the above-discussed spectra may be interpreted as resulting from two metal ion centers with $C_2$ symmetry generated by a distortion of the coordination environment from the idealized X-ray symmetry. The slight differences between the emission spectra may come from slightly different conformations induced by intramolecular interactions either because the microcrystals contain defects or because of hydrogen bonding with the solvent molecules (vide infra). The excitation spectrum at 295 K displays only one (broad) band and the corresponding emission (Figure S4, Supporting Information) may also be interpreted as arising from metal ions in low symmetry. When the temperature is increased (Figure 12 and Figures S5 and S6, Supporting Information), the emission spectra become broader, as expected from a larger contribution from vibronic

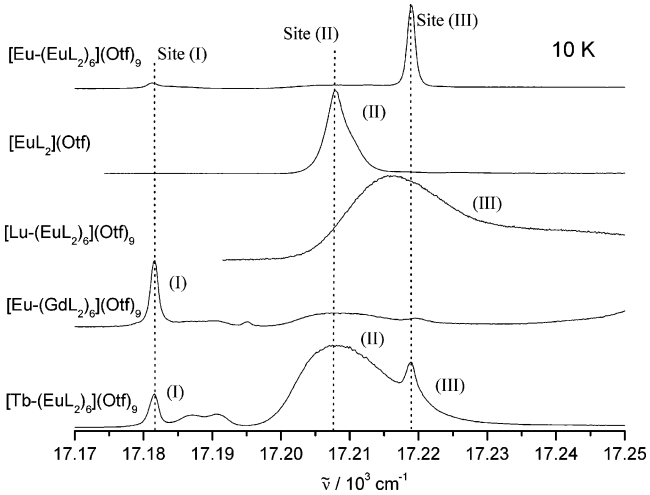


**Figure 13.** Excitation spectra at 10 K of the $[Ln\subset(LnL_2)_6](Otf)_9$ complexes (Ln = Eu, Lu, Tb, Gd) upon monitoring the Eu($^5D_0 \rightarrow {}^7F_2$) transition (large band analysis).

components. However, both excitation and emission spectra display sudden drastic changes at a given temperature, which differs depending whether the sample is cooled or heated, and these changes are reversible. The changes are observed between 240 and 230 K when the sample is cooled, but only at 290 K when the sample is heated. These modifications could be interpreted in terms of either a "phase transition" leading to a rearrangement of the coordination sphere of the peripheral ions or, more likely, the presence of energy-transfer processes between the peripheral and the central ions. Indeed the variable-temperature NMR studies indicate that the symmetry of the solution species remain unchanged in the temperature range of 243−343 K. Furthermore, X-ray diffraction measurements in the temperature range of 190−298 K show that the unit cell of $[Eu\subset EuL_2)_6](Otf)_9$ remains unchanged between 190 and 240 K, while the crystal decomposes at 298 K because of solvent loss.

To confirm the assignment of the $Eu^{III}$ sites, three heteropolymetallic rings have been synthesized, with peripheral $Eu^{III}$ ions in $[Lu\subset(EuL_2)_6](Otf)_9$ and $[Tb\subset(EuL_2)_6](Otf)_9$ or a central $Eu^{III}$ ion in $[Eu\subset(GdL_2)_6](Otf)_9$. Luminescence spectra show that the latter two samples are contaminated by the precursor complex $[EuL_2](Otf)$, particularly in the $Tb^{III}$ sample; the quantities of the monomeric complex depends on the exact synthesis conditions. Moreover, $Eu^{III}$ ions are detected in the other sites. Nevertheless, an analysis of the emission and excitation spectra is possible, and at low temperature, the excitation profile of the Eu($^5D_0 \leftarrow {}^7F_0$) transition was recorded by monitoring all of the most intense components of the $^5D_0 \rightarrow {}^7F_2$ transition (large-band excitation spectra). At low temperature (Figure 13), the $^5D_0 \leftarrow {}^7F_0$ excitation profiles display the central site I for $[Eu\subset(EuL_2)_6](Otf)_9$ and $[Eu\subset(GdL_2)_6](Otf)_9$, as well as $Eu^{III}$ in the periphery of the ring. With $[Lu\subset(EuL_2)_6](Otf)_9$, only emission from the peripheral site III is observed, as expected. Similar measurements have been performed at room temperature (Figure S7, Supporting Information), and the results are similar to those described for the homometallic complex, with the absence of site III. The emission spectra upon broadband or selective excitation display similar spectra (Figure S8 and S9, Supporting Information) for the different sites.

The luminescence lifetime of the $^5D_0$(Eu) excited-state measured at 10 K upon direct excitation (17 181 $cm^{-1}$, site I) amounts to 2.02 ms, while it decreases to 1.65−1.71 ms at 295 K (Table 5). Upon direct excitation (17 219 $cm^{-1}$, site III), they lie in the range from 1.71 to 1.74 ms, depending upon the excitation and analyzing energies. At room temperature, as the signal disappears, the Eu($^5D_0$) lifetimes could not be determined. All these lifetimes (1.6 ms for site II) point to the absence of water molecules in the inner coordination sphere, as confirmed by the X-ray structure. When the temperature is increased, they decrease to reach 1.7 ms for site I and 1.5 ms for site II. This relatively small temperature dependence may be rationalized on the basis of interactions with vibrations only, excluding photoinduced electron-transfer (PET) phenomena. Excitation through the $^1\pi\pi^*$ ligand state results in similar lifetimes, indicating a fast energy transfer from the ligand to the 4f states, like that for the homometallic complex.

The Eu($^5D_0$) lifetime of $[Lu\subset(EuL_2)_6](Otf)_9$ (site III) is interesting. It is larger than the ones measured in the other complexes (∼1.9 vs 1.7 ms), and more importantly, it can be measured at room temperature, at which it remains long (1.86 ms) This is indicative of the absence of Eu(III) ions in the central site of this compound (see excitation spectrum Figure 13).

Finally, quantum yields have been determined at room-temperature both for solid-state samples and for solutions in anhydrous acetonitrile. In the solid state, they amount to 10.7 and 24.9% for $[Eu\subset(GdL_2)_6](Otf)_9$ and $[Eu\subset(EuL_2)_6](Otf)_9$, respectively, while the solution values are close to 27% (23, 23, 30, and 32% for $[Eu\subset(TbL_2)_6](Otf)_9$, $[Lu\subset(EuL_2)_6](Otf)_9$, $[EuL_2](Otf)$, and $[Eu\subset(EuL_2)_6](Otf)_9$, respectively). Combined with the lifetime data, these values point to the disappearance of the emission of site III at room temperature being possibly caused by interactions or energy transfers between the $Eu^{III}$ ions in sites I and III.

## Conclusions

The assembly of heptametallic complexes from a monometallic precursor in rigorously anhydrous acetonitrile occurs only in the presence of an excess of noncomplexed Ln(III) cation, leading to highly organized structures in solution for the intermediate $Ln^{III}$ ions Eu−Tb for which the heptametallic assembly is the only species forming in solution. This species is also the major solution product for larger ions such as $Nd^{III}$ but its formation is not observed under similar conditions for the smaller lanthanide ions Y−Lu. Therefore, the assembly of such edifices requires the presence of an accessible coordination site at the center of the structure. The overall size of the cyclic assembly is controlled by the ionic radius of the lanthanide ion. NMR studies show that these highly organized ring structures are stable in solution and that there is no ligand exchange up to 343 K. High-resolution solid-state luminescence spectra of the homoheptametallic $Eu^{III}$ wheel point to the presence of two different

emitting sites with luminescence intensity displaying large temperature dependence. The rather long luminescence lifetime of the polymetallic complex in solution is very similar to the lifetime in the solid state in agreement with the presence of a rigid structure in solution and with the absence of interaction with solvent molecules. The quantum yield of the metal-centered the luminescence of the heptametallic complex in acetonitrile is similar to the value found for the precursor monomeric complex, suggesting that the cyclic arrangement of six $[EuL_2]$ components does not lead to intramolecular quenching effects as observed in trimetallic lanthanide helicates,[19] despite the shorter distance between neighboring $[EuL_2]$ units (6.25 Å) with respect to the intermetallic distance in the trimetallic helicates (9.0−9.3 Å). Therefore, the self-assembled nanosized ring structure described here is particularly well adapted for the inclusion of highly luminescent lanthanide centers. Work in progress in our laboratories aims at inserting different monomeric units in similar ring structures.

By exploiting the different size requirements of the two metal sites present in the cyclic structure, we have developed a rational synthetic method for the preparation of pure heteropolymetallic complexes. We selectively prepared $[EuL_2]_6$ rings hosting a smaller $Ln^{III}$ ion in their center. The high stability of the resulting heterometallic wheel associated with its high rigidity prevents scrambling of the metal ions between different sites and allows the isolation of pure heterodimetallic complexes. For $[Lu\subset(EuL_2)_6](Otf)_9$, high-resolution solid-state photophysical studies confirmed the presence of only one emitting site in agreement with the absence of distribution of the lutetium cation in the peripheral sites, as seen in the crystal structure determination. This heptametallic complex is the first example of selective assembly of two different lanthanide ions in a large polymetallic structure fully characterized both in solution and in the solid state. A large number of similar bimetallic combinations with different lanthanide ions inserted in a planned fashion in the peripheral sites can thus be predicted. The synthetic approach described here allows the isolation of various f−f′ heterometallic edifices. Although the two metal centers cannot be chosen at will, since the central site will only host smaller Ln(III) ions, it is anticipated that we will be able to assemble edifices possessing luminescent centers which emit both in the visible and in the near-infrared ranges, This type of polymetallic compounds is not only ideally suited for the study of intermetallic energy transfer processes but also as precursors for the development of lanthanide-based optical devices.

**Acknowledgment.** We thank Pierre Alain Bayle for help with NMR measurements, Colette Lebrun for the ES-MS measurements, and Frederic Gumy for his help in the luminescence measurements.

**Supporting Information Available:** Luminescence emission and excitation spectra (Figures S1−S8) and complete tables of crystal data and structure refinement, atomic coordinates, bond lengths and angles, anisotropic displacement parameters, and hydrogen coordinates for compounds **6**, **7**, and **10**. This material is available free of charge via the Internet at http://pubs.acs.org.

IC061806O